# The centroid of tree crowns as an indicator of abiotic processes in a balsam fir wave forest

ALEXANDER ROBERTSON

*Canadian Forestry Service, Newfoundland Forest Research Centre, Box 6028, St. John's, Nfld., Canada A1C 5X8*

Received September 8, 1986

Accepted March 4, 1987

ROBERTSON, A. 1987. The centroid of tree crowns as an indicator of abiotic processes in a balsam fir wave forest. Can. J. For. Res. **17**: 746–755.

Wave forests are rare and were previously known only in high altitude *Abies balsamea* forests in northeastern U.S.A. and in subalpine *A. veitchii – A. mariesii* forests in Japan. Wave forests have been discovered at several locations in Newfoundland, including a very large and unique wave forest extending over 100–150 km$^2$ on the coastal plain of northwestern Newfoundland. The wave fronts, characterized by dead tree strips, are mostly sinusoidal with an axis aligned in the direction of the prevailing wind, are spaced 100–150 m apart, and move in 55-year cycles. Crest-shaped wave fronts are concave on the windward side, occur as random events, and leave a trailing edge to the right of the prevailing wind that becomes a sinusoidal wave front. Two types of wave cycles, *uniform cycle* and *broken cycle*, have been identified as regular and random events, respectively. This paper reports the initial results of a detailed study on the impact of wind on the dynamics of a wave forest and concentrates on the centroid as a measure of crown asymmetry useful for distinguishing between purely biotic (mainly competition) and abiotic (mainly wind) processes as the primary cause of crown asymmetry. The development of wave forests at Spirity Cove is described based on the hypothesis that longitudinal helical roll vortices are primarily responsible for their formation.

ROBERTSON, A. 1987. The centroid of tree crowns as an indicator of abiotic processes in a balsam fir wave forest. Can. J. For. Res. **17** : 746–755.

Les forêts régénérées en vagues sont un phénomène rare dont l'existence a seulement été constatée auparavant dans les forêts d'*Abies balsamea* de haute altitude du nord-est des États-Unis et dans les forêts subalpines d'*A. veitchii – A. mariesii* au Japon. Des forêts régénérées en vagues ont été découvertes en plusieurs endroits au Terre-Neuve, y compris une très grande forêt régénérée en vagues unique sur la plaine côtière du nord-ouest de la Terre-Neuve, qui s'étend sur une superficie de plus de 100–150 km$^2$. La plupart des fronts des vagues, caractérisés par des bandes d'arbres morts, sont sinusoïdaux avec un axe aligné sur la direction du vent dominant, ont un espacement de 100–150 m et se déplacent en cycles de 55 ans. Les fronts des vagues en forme de crête sont concaves du coté du vent, sont des événements qui ont lieu au hasard et laissent un bord de fuite à droite du vent dominant qui devient un front de vague sinusoïdal. Deux types de cycles de vagues, *cycle uniforme* et *cycle rompu*, ont été identifiés respectivement comme des événements reguliers et qui ont lieu au hasard. Cette communication rend compte des résultats initiaux d'une étude détaillée de l'effet du vent sur la dynamique d'une forêt régénérée en vagues, et elle se concentre sur le centroïde comme une mesure de l'asymétrie des houppiers utile pour distginguer entre des processus purement biotiques (principalement la concurrence) et abiotiques (principalement le vent) comme la cause principale de l'asymétrie des houppiers. Une déscription du développement de forêts régénérées en vagues à Spirity Cove est donnée, basée sur l'hypothèse que des vortex de Goertler sont les causes principales de leur formation.



## Introduction

Wave forests are rare and were previously known only in high altitude balsam fir (*Abies balsamea*) forests of northeastern U.S.A. (Sprugel 1985) and in *A. veitchii – A. mariesii* forests on Mt. Shimagare and elsewhere in Japan (Oshima et al. 1958; Kimura 1982; Koyama and Fujita 1981). This paper records not only new locations but also a unique case of an extensive balsam fir wave forest on a low-lying coastal plain at Spirity Cove, northwestern Newfoundland (Fig. 1).

Classic examples of wave forests in Newfoundland occur mainly on steep slopes in coastal areas; e.g., Peter's River and Point La Haye on the southeast shore of St. Mary's Bay. Less obvious examples occur near Rocky Harbor in Gros Morne National Park and in the vicinity of Daniel's Harbor south of Spirity Cove. The wave forest at Spirity Cove is the most extensive ever recorded, extending over an area of 100–150 km$^2$ on flat to gently sloping terrain. Figure 2 shows a section of the wave forest at Spirity Cove, plus a sketch of the distribution of sinusoidal and crested wave fronts. Figure 3 is a schematic diagram showing a series of wave cycles and some basic statistics of an average wave profile.

Because they occur in regular cycles, wave forests are of considerably scientific and practical importance (Sprugel 1985), not the least of which is the impact of wind on forest dynamics. This paper reports the initial results of a detailed study to determine the aerodynamic principles most responsible for the formation of the Spirity Cove wave forest. The principle variables studied include the orientation of centroids of tree crowns, wave fronts and wind-thrown trees in relation to wind

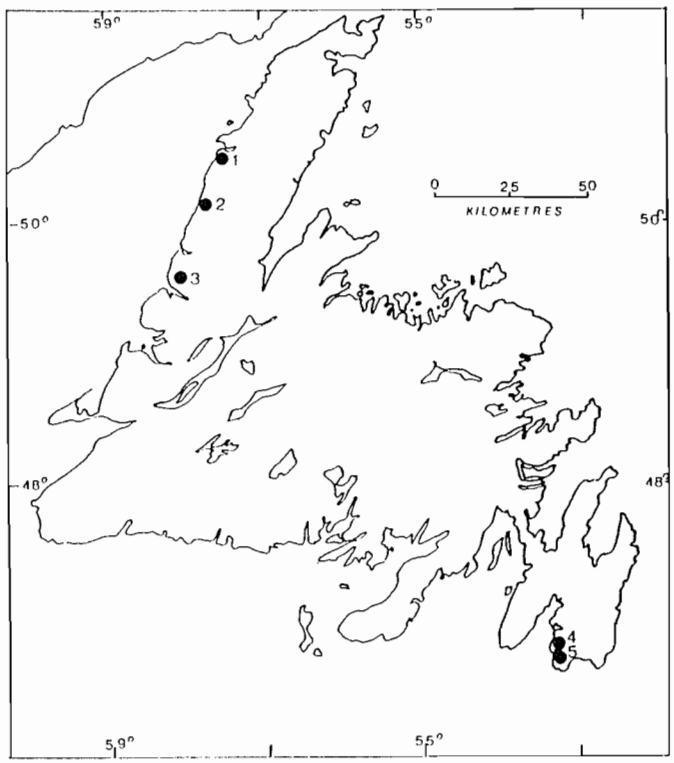


FIG. 1. Map of Newfoundland showing location of balsam fir wave forests. 1, Spirity Cove; 2, Daniels Harbor; 3, Rocky Harbor; 4, Peter's River; 5, Point La Haye.

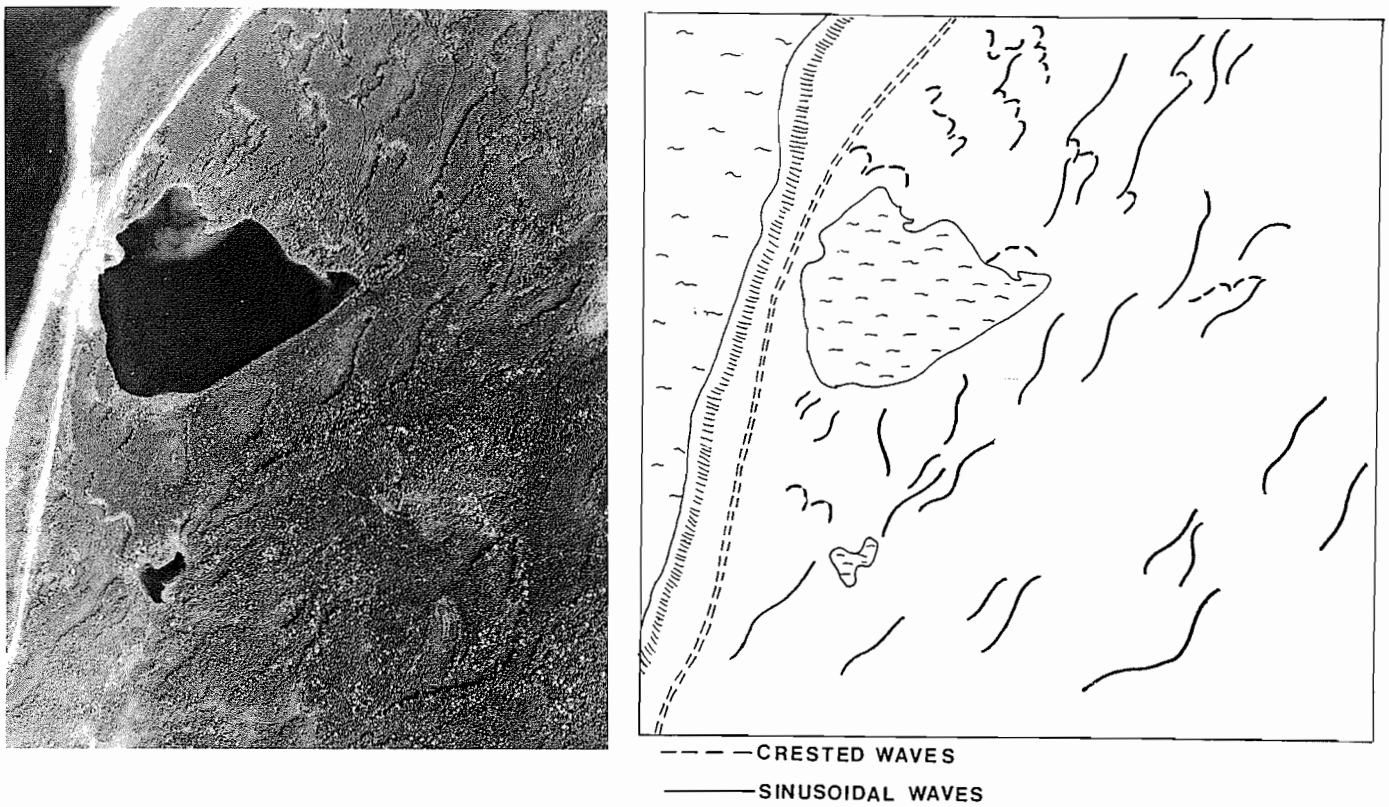


FIG. 2. (A) Aerial photo of wave forests at Spirity Cove, Newfoundland. (B) Map showing the distribution of sinusoidal and crested wave fronts.



data. Since this involves directional data, the principles of circular statistics is the main analytical tool for examining the relationship between wind and wave forests.

## Methods

Three consecutive wave profiles were sampled. Four plots were established equidistant through each wave cycle as shown in Fig. 4. The A and B plots, and C plot in wave 3, represent the taller sections of the profiles and were 2 × 10 m and aligned parallel with the wave front; the remaining C and D plots were 2 × 5 m and also aligned parallel with the wave fronts. One hundred and twenty trees, 10 from each plot, were randomly selected to represent the percentage frequency of all diameter classes.

The measurements pertinent to this paper included crown base spread and crown length in north, east, south, and west directions, and total dry weight of crowns.

*The centroid*

The centroid of tree crowns was derived by first estimating the volume and mass of four crown sections and calculating the vector coordinates of each section; viz., northeast, southeast, southwest, and northwest, respectively. Thus the total crown volume ($V$) was estimated by

$$[1] \quad V = \sum_{i=1}^{4} v_i$$

where $v_i$ = (sectional crown basal area × length)/3. Given the total crown weight ($B$), the proportion of crown weight in each section ($b_i$) was estimated from

$$[2] \quad b_i = (v_i/V)B$$

The crown centroid ($C$), weighted by crown weight, was calculated from

$$[3] \quad C = 1/B\left(\sum_{i=1}^{4} b_i\, c_i\right)$$

where $c_i$ is the Cartesian coordinates of the vectors of each crown section, i.e.,

$$[4] \quad c_i = x_i/3,\ y_i/3$$

The Cartesian coordinates ($x_c$ and $y_c$) of the crown centroid ($r_c$) are located by

$$[5] \quad x_c = 1/B\left(\sum_{i=1}^{4} x_i\right), \qquad y_c = 1/B\left(\sum_{i=1}^{4} y_i\right)$$

By transformation, the polar coordinates of the vector length of the crown centroid ($r_c$) are obtained from

$$[6] \quad r_c = [(x_c)^2 + (y_c)^2]^{0.5}$$

and its angle ($\phi_c$) determined from one of the following relevant equations:

$$[7] \quad \begin{aligned} \phi_c &= \tan^{-1}(x/y) && (x>0, y>0)\\ \phi_c &= \tan^{-1}(|y|/x) + 90^\circ && (x>0, y<0)\\ \phi_c &= \tan^{-1}(|y|/|x|) + 180^\circ && (x<0, y<0)\\ \phi_c &= \tan^{-1}(|x|/y) + 270^\circ && (x<0, y>0) \end{aligned}$$

Exceptional cases are

$$[8] \quad \begin{aligned} \phi_c &= 90^\circ && (x=0, y>0)\\ \phi_c &= 270^\circ && (x=0, y<0)\\ \phi_c &= \text{Indeterminate} && (x=0, y=0) \end{aligned}$$

The polar coordinates of the mean vector length ($\bar{r}$) are calculated

$$[9] \quad \bar{r} = \left(\sum_{i=1}^{n} \cos\phi_c\right) + \left(\sum_{i=1}^{n} \sin\phi_c\right)$$

and mean vector angle ($\bar{\phi}$) calculated from either of the two equations

$$[10] \quad \begin{aligned} \bar{\phi} &= \tan(y/x) && \text{MOD } 360^\circ\ (x>0)\\ \bar{\phi} &= \tan^{-1}(y/x) + 180^\circ && (x<0) \end{aligned}$$

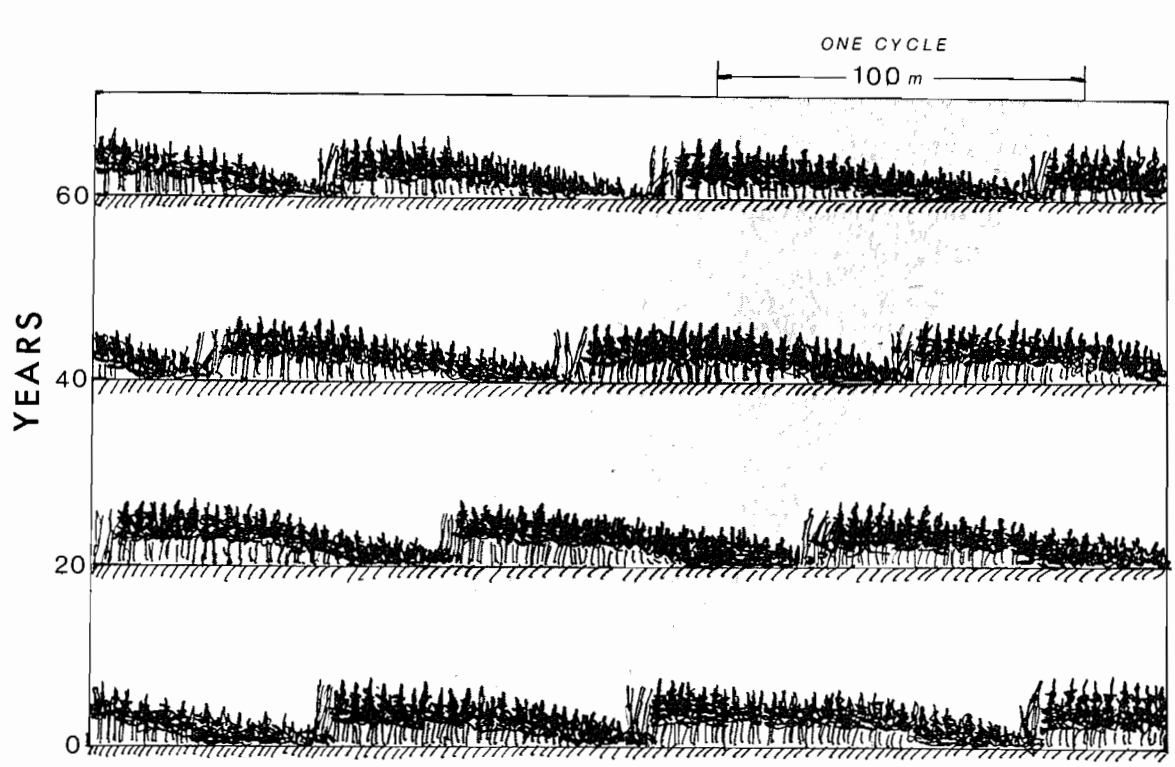


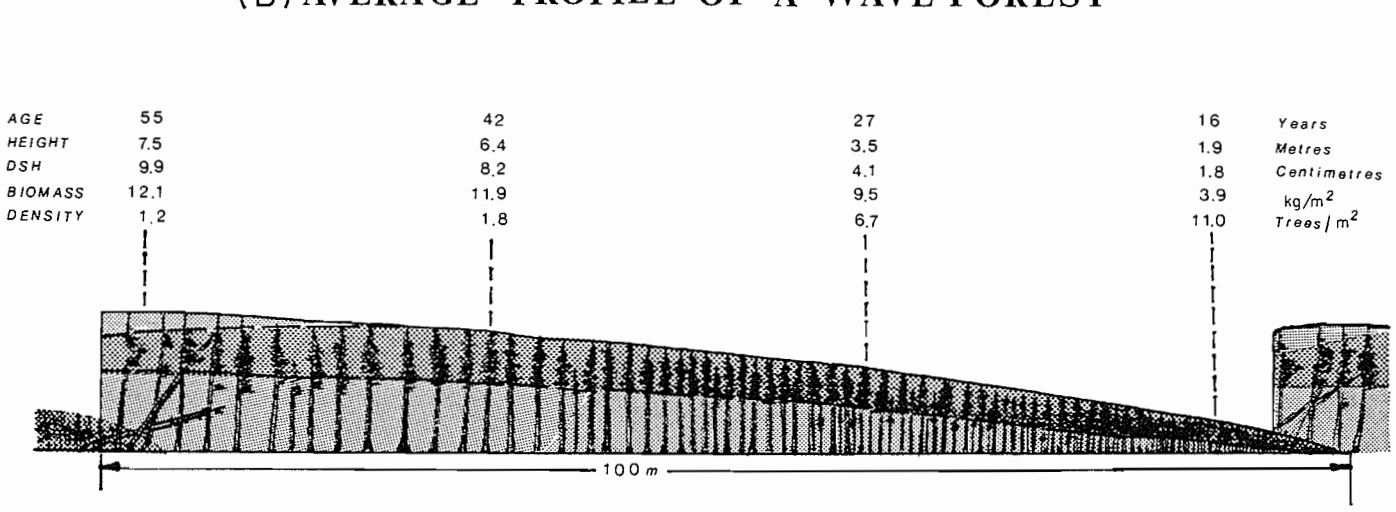


FIG. 3. (A) Profile of a balsam fir wave forest cycle. (B) Statistics of an average wave forest profile at Spirity Cove.

*Statistical analysis*

Because the analysis involves directional data, circular statistical techniques were used almost exclusively. The angular deviation ($\sigma°$) introduced by Batschelet (1965) is defined as

$$[11] \quad \sigma° = (180°/\pi) \times [2(1 - r)]^{0.5}$$

The appropriate confidence interval ($\delta°$) is obtained from charts in Batschelet (1983), which are based on the work of Stephen (1962) and Brown and Mewaldt (1968).

Since the length of the mean vector ($r$) ranges from 0 to 1, it is used to measure the strength of directionality. Also, if $\bar{r} < r(\alpha)$ the null hypothesis of randomness cannot be rejected; conversely, if $\bar{r} > r(\alpha)$ then directionality exists, and the greater the value of $r$ the more concentrated is directionality. These basic statistics, $\bar{r}$, $\sigma°$, and the confidence level (at 95% probability), and the critical value range, with respect to angular observations, are illustrated in the statcircle (Fig. 5). The statcircle may also include a significance test dissector as an additional but less powerful visual aid for estimating significance. The dissector is a modification of Hodges–Ajnes $V$-test by Batschelet. This modification is a two-sided test considering both tails of a binomial distribution and appropriate statistical tables can be found in Batschelet (1983). In the $V$-test, the lower the number of observation on one side of the dissector the more directional is the data.

The directedness of centroids in various plot categories was tested by

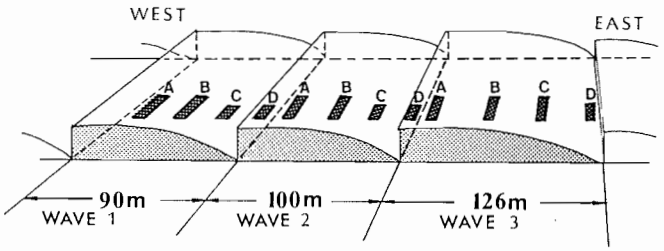


FIG. 4. Schematic diagram showing the length of three consecutive wave forest profiles sampled and the general location of sampling plots within each profile.

Moore's nonparametric test of directionality (Moore 1980). This is a second-order test taking into account both the mean vector length ($\bar{r}$) and mean vector angle ($\bar{\phi}$) and is defined by

$$[12] \quad D^* = D/n^{1.5}$$

where

$$[13] \quad D = \left[\left(\sum_{i=1}^{n} t_i \cos \bar{\phi}_i\right) + \left(\sum_{i=1}^{n} t_i \sin \bar{\phi}_i\right)\right]^{0.5}$$

$\bar{\phi}$ is continuous and $t_i$ is the rank of $\bar{r}$ from the smallest to the largest of corresponding $\bar{\phi}_i$ values. Directionality is established if Moore's statistic ($D^*$) exceed the critical value, i.e., $D^* > D^*(\alpha)$.

Mardia's Uniform test score (Mardia 1970; Mardia and Spurr 1973) was used to test for differences between the three wave profiles sampled. This test is particularly appropriate because the samples of grouped data is small and none of the angles of the mean centroids is coincidental. Mardia's statistic ($M^*$) is obtained from

$$[14] \quad M^* = 2\sum_{i=1}^{n} R_i^2/N_i$$

where $R_i^2$ is the vector length of each sample, i.e.,

$$[15] \quad R_i^2 = \left(\sum_{j=1}^{N} \cos \beta_{ij}\right) + \left(\sum_{j=1}^{N} \sin \beta_{ij}\right)$$

$\beta_{ij} = \bar{\phi}_{ij}\,\theta$, with $\bar{\phi}_{ij}$ being the sequence of ranks of the mean angles $\bar{\phi}_i$ from $j = 1,2, \ldots N$ and $\theta$ is the respacing of sample angles into multiples of $\theta = 360°/N$. Mardia and Spurr (1973) and Batschelet (1983) provide three-sample statistical tables for $M^*$. However, since $M^*$ is approximately distributed as $\chi^2$, with $2(n - 1)$ degrees of freedom, then $\chi^2$ tables can be used to compare $M^*$ with $M^*(\alpha)$.

## Results

The plot categories, A, B, C, and D of a typical wave cycle represent four stages of development: A, decadent, wind-thrown gaps in the canopy and severe crown loss on standing trees at fairly regular spacing; B, mature, light self-thinning with widely separated wind-shaped symmetric crowns and more or less randomly distributed trees; C, immature, moderate to high self-thinning with barely contiguous crowns shaped mainly by competition, and moderately clustered tree distribution; D, regeneration, strongly self-thinning with contiguous crowns forming a dense canopy with very clustered tree distribution.

The statistics of the crown centroids is summarized in Table 1, with $n = 30$ for each plot category. Figure 6 shows the Cartesian coordinates of sample tree centroids and corresponding statcircle for each plot category.

Figure 7 is a plot of Mardia's nonparametric test for directionality comparing the difference between wave cycles. The calculated value of Mardia's statistic ($M^*$) is 1.536; therefore, with $M^* > M^*(\alpha)$ at 0.05 significance level, there is no difference between wave cycles. In other words, there is a clear indication that the degree of directedness of centroids is constant with respect to plot categories within each wave cycle.

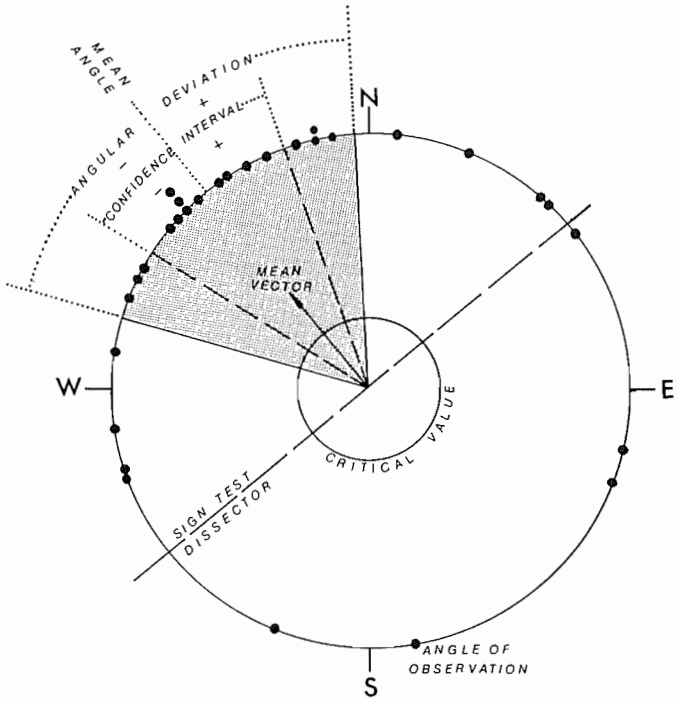


FIG. 5. A statcircle: a convenient graphical summary of various circular statistics and tests of significance pertaining to directional data in this study (see text for derivation of statistics).

TABLE 1. Analysis of the directionality of the centroids of tree crowns in a balsam fir wave forest at Spirity Cove, Nfld.

| Plot category | Mean age (years) | $\bar{r}$ | $\bar{\phi}$ (°) | $\sigma$° (°) | $\delta$° (°) | $D^*$ | $k$ |
|---|---|---|---|---|---|---|---|
| A | 55 | 0.42 | 293 | 61.7 | 35 | 1.18** | 4*** |
| B | 42 | 0.55 | 317 | 54.3 | 25 | 1.52*** | 4*** |
| C | 27 | 0.28 | 12 | 68.8 | 61 | 0.6 | 11 |
| D | 16 | 0.26 | 283 | 69.7 | 76 | 0.7 | 10 |

NOTE: $\bar{r}$, mean vector length; $\bar{\phi}$, mean vector angle; $\sigma$°, angular deviation; $\delta$°, confidence level at 95% probability; $D^*$, Moore's statistic; $k$, significance test statistic. **, 0.01 level of significance; ***, 0.001 level of significance.

At 10 years of age, near the beginning of the cycle, the stand density ranges from 80 000 to 140 000 stems ha$^{-1}$. Because canopy closure is complete at this stage wind cannot penetrate the stand to any great extent. Consequently, wind has little effect on the saplings, except perhaps on those dominants that grow well above the main canopy. Generally, the centroids, as a group, are distributed randomly (i.e., they exhibit no directionality). Therefore, self-thinning through vigorous competition is perceived to be the dominant process causing asymmetry over the first 30% of a wave cycle.

Gradually, over the next 60% of a wave cycle, excessive tree sway, where the lower parts of the crowns are constantly beating against neighbouring crowns, plus rime and salt from sea spray causes severe branch loss. Self-thinning in this case results more from abiotic than biotic processes and the crowns gradually become oriented in a northwesterly direction as deformation becomes severe. Wind throw at this stage is still quite rare.

The last 10% of a wave cycle is characterized by highly directional crown deformation, dieback, and, at the outer edge, skeletons of broken, standing dead trees (stripped of branches and bark and bleached by the elements) and wind-thrown derelicts. Under the standing and wind-thrown dead trees there

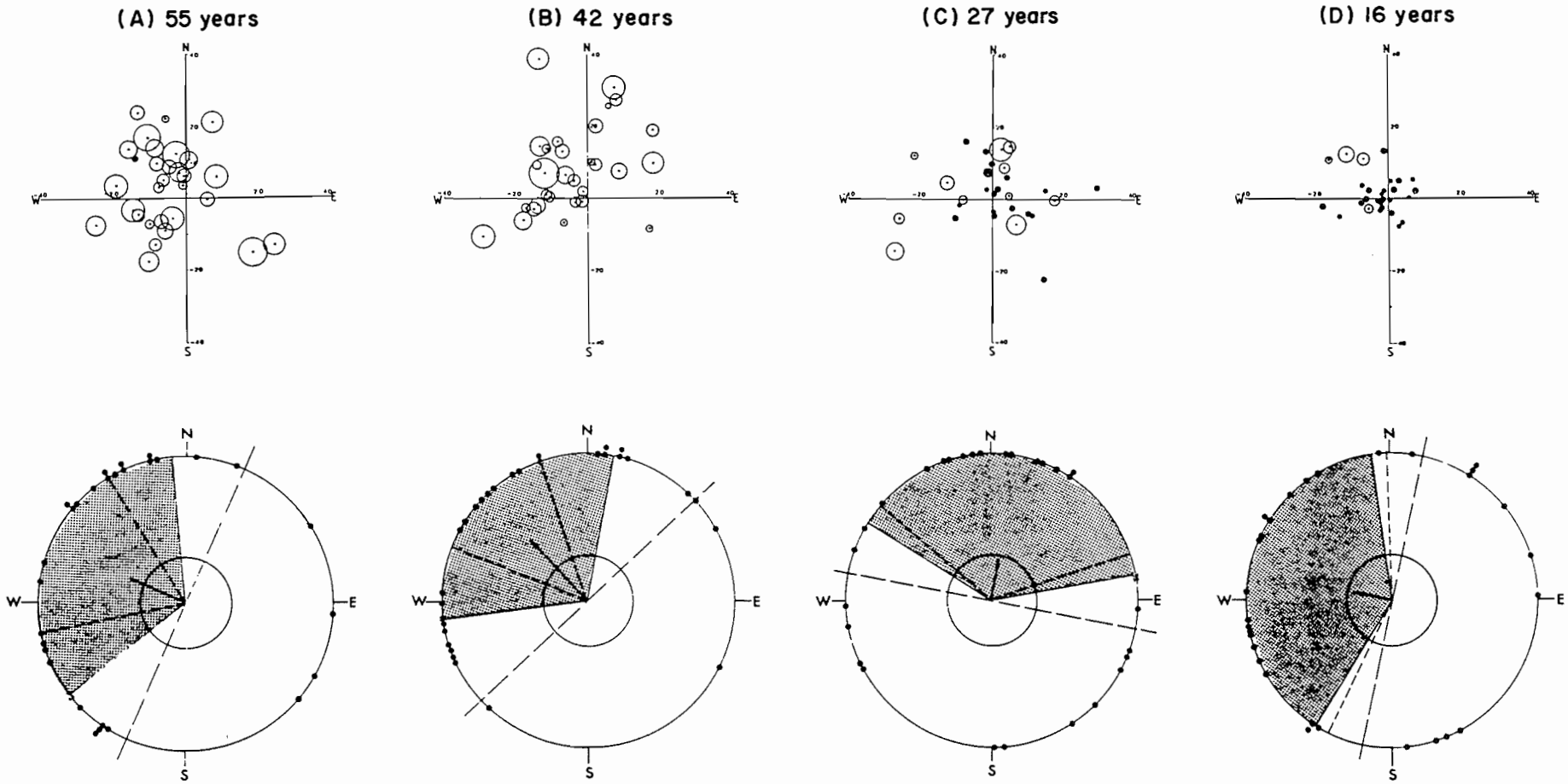


FIG. 6. The cartesian coordinates of crown centroids of sample trees in four plot categories (top); the intersection of the four principle points of the compass represents the centre of the stem and the open circles are scaled to show the diameter (stump height) classes. The corresponding statcircle (below) shows the transformation of cartesian coordinates into polar coordinates to summarize directionality as shown in the previous figure.

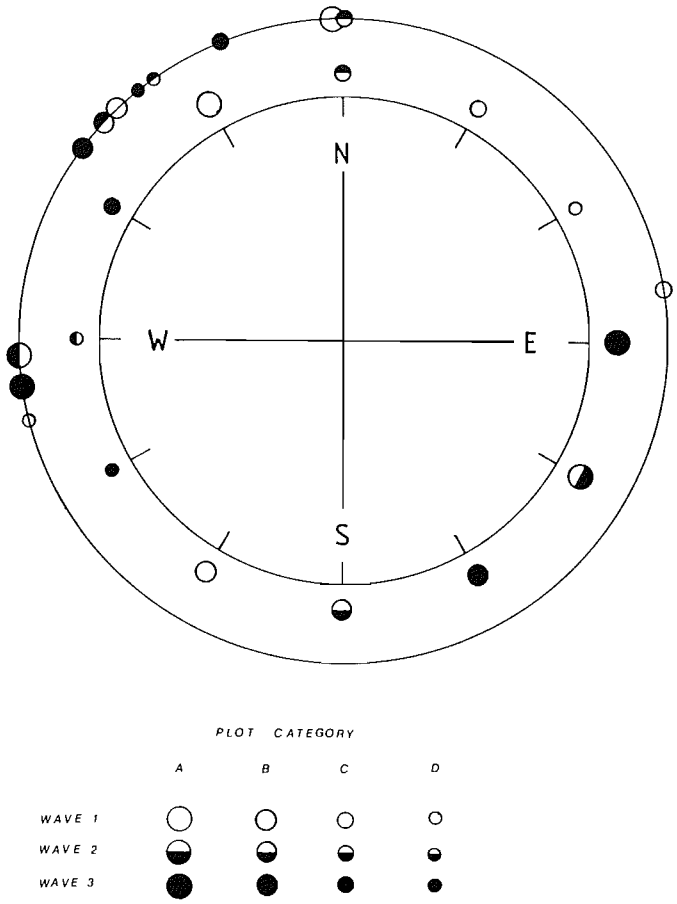


FIG. 7. Diagram of Mardia's nonparametric test for differences in directionality between the angle of centroids in three consecutive wave profiles sampled. The outer circle shows the distribution of the mean angle of crown centroids in each plot category in three wave profiles; the inner circle is a respacing of these angles by 360 divided by the number of observations (in this case 12) to obtain Mardia's statistic ($M^*$) (see text for details).

is an abrupt change in the ground flora from a moss carpet of *Hylocomnium splendens* and *Pleurozium schreberi* with a few herbs (*Cornus canadensis*, *Maianthemum canadense*, and *Clintonia borealis*) to dense balsam fir regeneration and occasionally small clumps of mountain birch seedlings (*Betula papyrifera* var. *cordifolia*) and, infrequently, white spruce (*Picea glauca*) and black spruce (*P. mariana*) seedlings.

The major axis of open growing tamarack (*Larix laricina*) tree crowns in the area lies in the direction of the prevailing wind, i.e., southwest to northeast (Robertson 1986). In the wave forest, however, mean crown deformation attributed to wind has a distinctive northwesterly trend. Obviously, the deposition of salt spray and rime (in winter) contribute significantly to crown deformation. However, since patterns of salt and rime deposition are governed by aerodynamics, it appears that eddies, akin to corner vortices, are responsible for shaping of crowns in the older stages of wave cycles. The evidence is based on the fact that, on the whole, most of the crown damage occurs on the south, east, and north sections of the crowns.

Figure 8 shows the frequencies of wind speed and direction during summer and winter at Daniel's Harbor (the nearest meteorological station to Spirity Cove with long-term records). Figure 9 shows seasonal vector wind speed at the same station. The close correlation between the prevailing wind and wave

TABLE 2. Orientation of wave forest fronts at Spirity Cove, Nfld.

| Shape of wave front | Axis | $n$ | $\bar{r}$ | $\bar{\phi}$ (°) | $\sigma$° (°) | $\delta$° (°) |
|---|---|---|---|---|---|---|
| Crested | Minor | 14 | 0.97 | 48 | 14.0 | 6.0 |
| Sinusoidal | Major | 31 | 0.96 | 33 | 16.2 | 4.5 |

NOTE: $n$, number of wave fronts; $\bar{r}$, mean vector length; $\bar{\phi}$, mean angle; $\sigma$°, angular deviation; $\delta$°, confidence interval at 95% probability.

forest formation is reflected in a number of ways: (*i*) the direction of wind-thrown trees in the dead tree strips coincides with the winter vector winds (Fig. 10) and (*ii*) the orientation of the major axis of sinusoidal wave fronts and the minor axis of crested wave fronts coincides with the summer vector winds (Fig. 11, Table 2).

## Discussion

According to prevailing hypothesis, wave forests originate from gaps in a more or less uniform mature stand. Iwaki and Totsuka (1959) give a hypothetical diagram showing how wave forests are supposed to have developed from several gaps, which enlarge into crest-shaped waves that ultimately merge to form a long dead-tree strip. Sprugel (1976) essentially supports the "gap theory," but notes that trees are already dead before being wind thrown. A feature lacking in the "gap theory" is an associated aerodynamic principle that would establish and maintain a wave forest.

An alternative hypothesis, which I will call the "vortex theory," emphasizes that gaps may not be necessary in wave forest formation, although they are important in certain cases such as the creation of crested waves. Also, the theory implies that wave forests are a manifestation of an aerodynamic phenomenon called Goertler vortices (also known as longitudinal helical roll vortices).

The "vortex theory" accounts for two types of wave formations (although neither are mutually exclusive); viz., uniform cycle and broken cycle. The uniform cycle is characterized by sinusoidal wave fronts which move parallel to the direction of the prevailing wind in virtually predictable cycles (Fig. 12*a*). Such a cycle will prevail for generations and perhaps even centuries providing there are no major disturbances. The broken cycle, on the other hand, is a manifestation of disturbances similar to those of the "gap theory." Evidently, crested wave fronts almost always originate from gaps created at the edge of sinusoidal wave fronts. Such gaps are caused either by a deeper penetration of wind throw owing to storm winds or the death of a large birch tree, which are known to create "early gaps." Over time these gaps enlarge into crested wave fronts that move upwind in the direction of the prevailing wind flow. Occasionally, crested wave fronts move independently of sinusoidal wave fronts; however, usually the movement of a crested wave is synchronized with a sinusoidal wave front as shown in Fig. 12*b*. In either case, a sinusoidal wave will reform behind a crested wave on the right of the major axis of the original sinusoidal wave front. Crested wave fronts normally leave a trailing edge on its right side, which in effect becomes a short, intermediate sinusoidal wave front. Hence, after a crested wave has run its course the whole system will settle back to a uniform cycle until further disruption.

The existence of a uniform cycle as the dominant formation and the directionality of crown centroids suggests that vortex streets may be the underlying aerodynamic principle responsible for the formation of wave forests at Spirity Cove. That crested

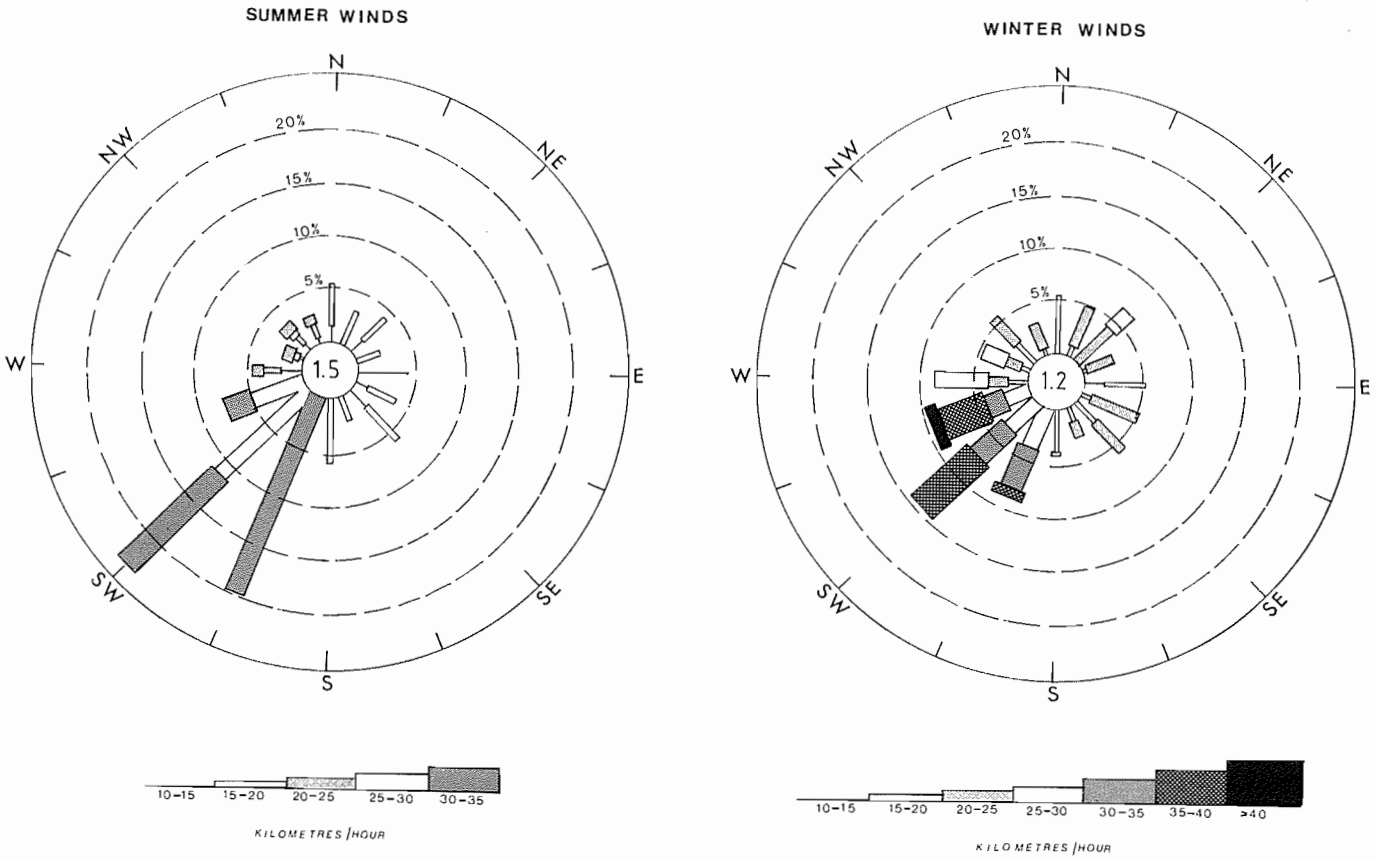


FIG. 8. Frequency of summer (May–September) and winter (October–November) wind speed and direction at Daniel's Harbor, Newfoundland (data source: Atmospheric Environment Service, Canadian normals, 1951–1980).

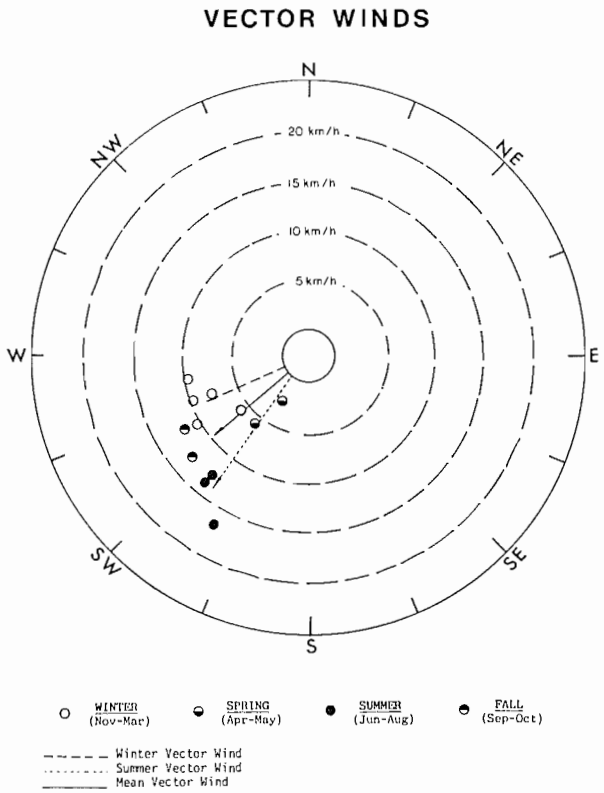


FIG. 9. Vector winds for Daniel's Harbor, Newfoundland (data source: Atmospheric Environment Service, Canadian normals, 1951–1980).

waves consistently leave a trailing edge on the right side of the prevailing wind is further indication of vortices. The type of vortices that are most likely to account for the regularity of uniform cycle are Goertler vortices (also known as longitudinal helical roll vortices), or a variation of them.

The existence of Goertler vortices has been established by hydrodynamic theory in the laboratory (Brunt 1937; Goertler 1940; Barnett 1972; Weihs 1973). Various phenomena associated with Goertler vortices are cloud bands (Angell et al. 1968; Kuettner 1971), turbulence over water (SethuRaman 1979), windrows of seaweed on the ocean surface (Faller and Woodcock 1964), smoke transport over the ocean (Woodcock and Wyman 1947), the formation of longitudinal sand dunes (Hanna 1969), and the soaring of gulls (Woodcock 1940). With respect to the flight of birds, one of Leonardo da Vinci's drawings[1] illustrates the trochoidal flight path of birds in helical roll vortices; undoubtedly, this is the first detailed reference to such vortices. Mathematical models pertaining to Goertler vortices are given by Goertler (1957), Kuettner (1971), and Hanna (1969).

In the formation of longitudinal sand dunes, which are a major landform in most of the large deserts, high surface temperatures result in convective strips. These convective strips are aligned in the direction of the prevailing wind and create Goertler vortices (Hanna 1969). Conversely, the sea–land interface differs from the deserts in that the cool Labrador Current, which flows up the west coast of Newfoundland, and the forest cover dampens convection. However, as Goertler

[1]CODEX ATLANTICUS, *folio 308 r-b*, Ambrosia Library, Milan.

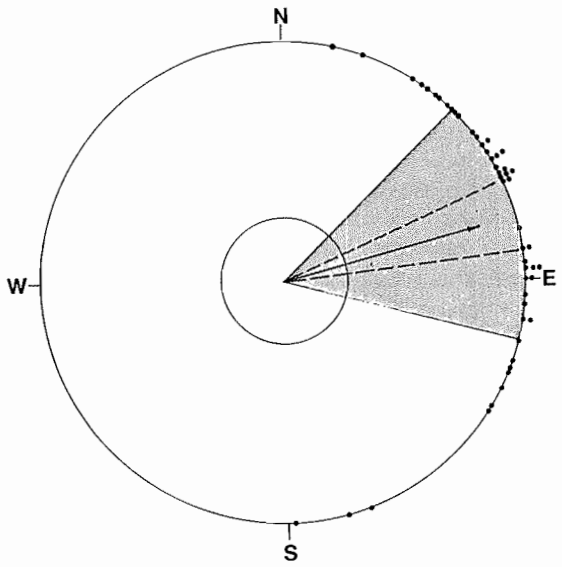


FIG. 10. Statcircle and photograph showing the strong directionality of wind-thrown trees in the "dead-tree" strips.

(1957) has shown, convection is not a prerequisite for the formation of Goertler vortices because of the equivalence between inertia and buoyant forces in creating this type of instability. This means that a cool, moist vortex would move downwards owing to the weight of its air mass as opposed to the hot, dry vortices that create longitudinal sand dunes.

Furthermore, helical vortices move in space with a relatively constant speed if the core radius also remains constant; otherwise, their speed increases with decreasing core radius. The conditions necessary for the formation and stabilization of Goertler vortices are as follows: a flat underlying terrain; a moderate wind with little variation in speed and direction; and a strong curvature of the wind profile. Such conditions prevail at Spirity Cove: e.g., in the direction of the prevailing wind there is a "fetch" of several hundred kilometres over the Gulf of St. Lawrence; the wind frequency diagrams show a consistent moderate wind regime. Figure 13 is a hypothetical diagram of the relationship between wave forest cycles and helical roll vortices. The classic Eckman Spiral is implied by the angle of the longitudinal axis of helical roll vortices in relation to the direction of the Geostrophic wind.

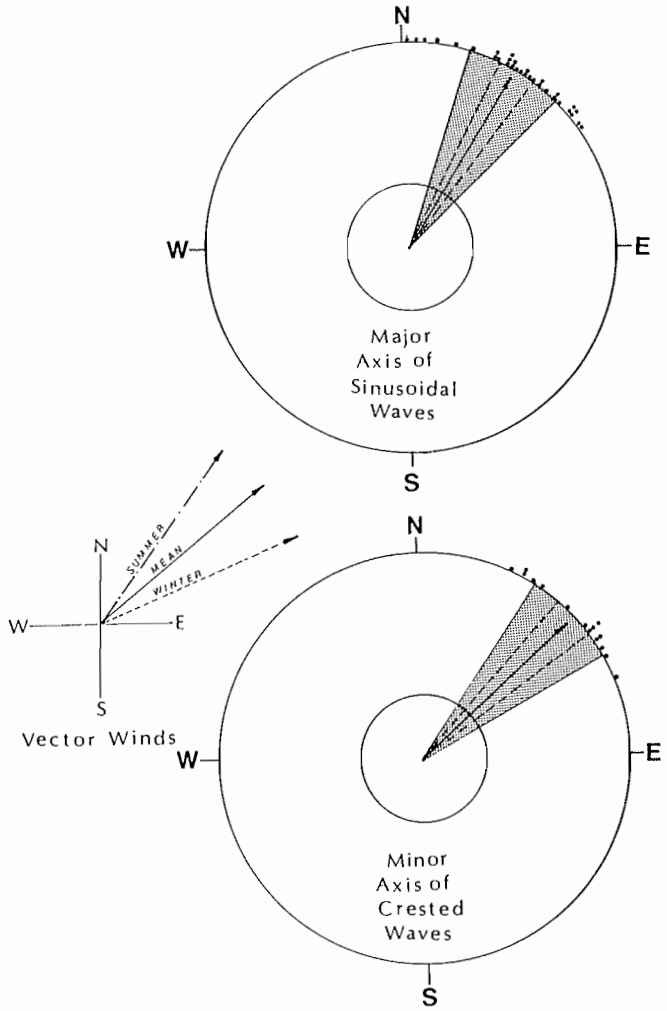


FIG. 11. Statcircle emphasizing the strong directionality of sinusoidal and crested wave fronts in relation to the direction of vector wind flow. In this case the vector wind direction is flowing to the northwest as opposed to flowing from the southwest as shown in Fig. 9.

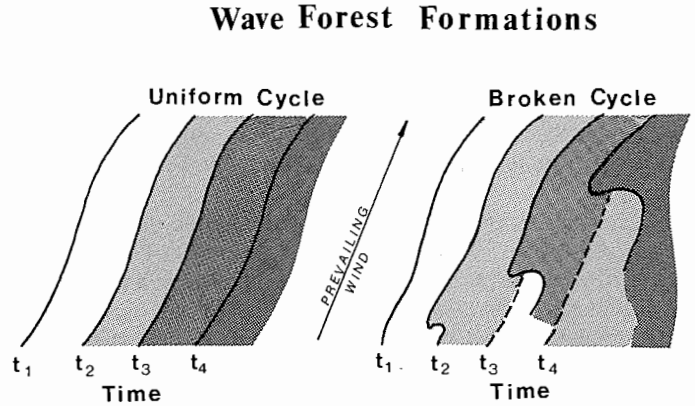


FIG. 12. Schematic diagram of two types of forest wave cycles at Spirity Cove. The uniform cycle, characterized by sinusoidal wave fronts, moves parallel to the direction of the prevailing wind and may prevail for several generations and even centuries. The broken cycle, characterized by sinusoidal waves broken up by crested wave fronts; crested wave fronts evolve from gaps at, or near, the edge of sinusoidal waves; in most cases, sinusoidal wave fronts will reform behind the crested wave fronts as they progress upwind.

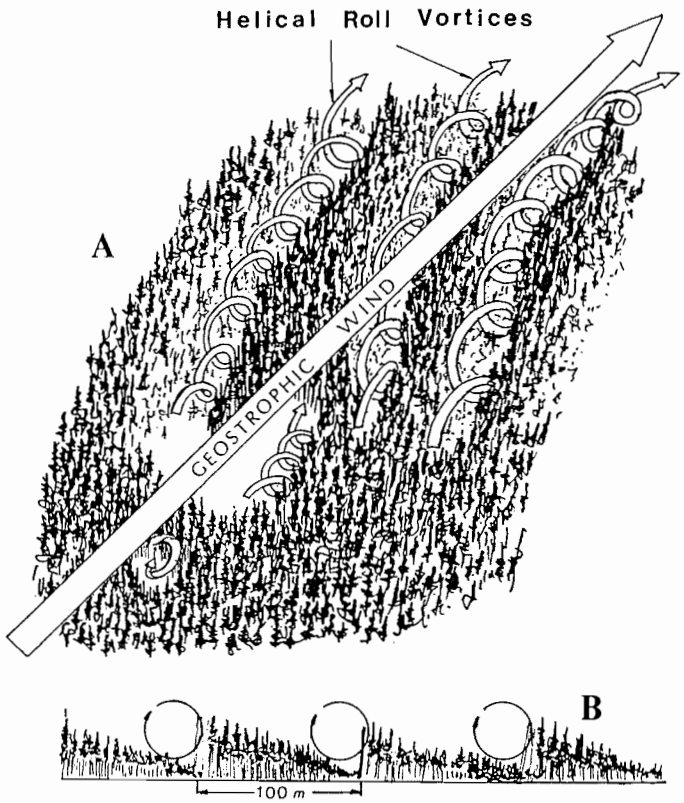


FIG. 13. Hypothetical diagram illustrating the aerodynamic mechanism by which helical roll vortices form wave forests. The angle of the major axis of the helical roll vortices in relation to the geostrophic wind direction implies the classic Eckman Spiral.

## Conclusions

The centroid of tree crowns is a useful measure for distinguishing between abiotic and biotic processes as the primary causes of crown asymmetry. In the early stages of a forest wave cycle crown asymmetry is controlled mainly by competition for light. In later stages of a wave cycle, crowns suffer from persistent winds that cause both mechanical damage from tree sway and, in winter, glaze and rime deposition and chemical damage from sea-salt spray. The cooling effect of the Labrador Current on the boundary layer also has a considerable impact by reducing primary productivity during the growing season. The directionality of the centroids indicate that eddies akin to corner vortices are primarily responsible for shaping the crown in the older stages of a wave cycle but have little effect in the younger stages.

Because standing dead trees are virtually the only ones that are wind thrown, wind throw is not thought to be a primary cause of wave forest formation because the age of a mature tree in an average wave cycle (55–60 years) is not significantly lower than the life-span of mature balsam fir in Newfoundland in general. However, wind throw in the dead tree strips is important in creating a specific pattern of environmental conditions conducive to mass regeneration necessary to maintain the cycle.

There is a high correlation between the prevailing wind direction and the directionality of the crown centroids controlled by abiotic processes, the orientation of wave fronts, and wind throw. The centroid of tree crowns are oriented 90° to the right of the prevailing wind. Sinusoidal wave fronts move parallel, while crested wave fronts move perpendicular to the summer vector wind direction. Wind-throw patterns are oriented parallel to the winter vector wind direction.

A "vortex theory" is proposed based on the belief that Goertler vortices, or a variation of them, may be responsible for the formation of wave forests at Spirity Cove. The theory precludes the necessity of gaps in a mature, uniform stand as a prerequisite for wave formation. Instead, bands of crown mortality, resulting from environmental stress controlled by aerodynamic features, suggests that wave forest formation could originate in immature stages of stand development. Two types of wave cycles have been identified. Uniform cycles, characterized by sinusoidal wave fronts, are regular events lasting several generations and perhaps even centuries; these move parallel to the prevailing wind direction. Broken cycles are characterized by a disruption of sinusoidal wave fronts by unusually large gaps created at, or near, the edge of the sinusoidal wave front either by wind throw or, occasionally, by the death of a large birch tree. These gaps are enlarged into crested waves that move upwind either synchronously with or, less often, independently of the sinusoidal wave front. As the crested wave fronts progress, sinusoidal waves reform behind them more or less on the same axis as the original sinusoidal wave, while short, intermediate sinusoidal waves are also created on a trailing edge on the right side of the advancing crested waves.

## Acknowledgements

This study was supported by the Canadian Forestry Service, Newfoundland Forest Research Centre, St. John's, Newfoundland. Special thanks go to Calvin French for his valuable assistance. Michael Roy, District Vocational School, Corner Brook (formerly of Port Saunders), and Ed Stewart, Department of Lands and Forests, Port Saunders, gave valuable logistical support during field work. I am indebted to the anonymous referees for their comments and suggestions. I also wish to thank Dr. P. S. Savill and R. A. Plumptre, Oxford Forestry Institute, University of Oxford, for their guidance throughout my D.Phil. studies.

ANGELL, J. K., PACK, D. H., and DICKSON, C. R. 1968. A Lagrangian study of helical circulation in the planetary boundary layer. J. Atmos. Sci. **28**: 707–717.

BARNETT, K. M. 1972. A wind tunnel experiment concerning atmospheric vortex streets. Boundary-Layer Meteorol. **2**: 427–443.

BATSCHELET, E. 1965. Statistical methods for the analysis of problems in animal orientation and certain biological rhythms. American Institute of Biology, Washington, DC.

——— 1983. Circular statistics in biology. Academic Press, London.

BROWN, T. L., and MEWALDT, L. R. 1968. Behaviour of sparrows of the genus *Zonotrichia* in orientation cages during the lunar cycle. Z. Tierpsychol. **25**: 668–700.

BRUNT, D. 1937. Natural and artificial clouds. Q.J.R. Meteorol. Soc. **63**: 277–288.

FALLER, A. J., and WOODCOCK, A. H. 1964. The spacing of windrows of *Sargassum* in the ocean. J. Mar. Res. **22**: 22–29.

GOERTLER, H. 1940. Uber eine dreidimensionale Instabilitat laminarer Grenzschichtstromungen an konkaven Wanden. Nachr. Ges. Wiss. Goettingen, Math. Phys. Kl. Neue Folge 1,2.

——— 1957. Uber eine Analogie zwischen den Instabilitaten laminarer Gunzschichtstromungen an konkaven Wanden und an erwarmten Wanden. Ing. Arch. **28**: 71–77.

HANNA, S. R. 1969. The formation of longitudinal sand dunes by large helical eddies. J. Appl. Meteorol. **8**: 874–883.

IWAKI, H., and TOTSUKA, T. 1959. Ecological and physiological studies of Mt. Shimagare. II. On the crescent-shaped "dead-tree"

strips in the Yatsugatake and Chichibu Mountains. Bot. Mag. **72**: 255–260.

KIMURA, M. 1982. Changes in population structure, productivity and dry matter allocation with the progress of wave regeneration of *Abies* stands in Japanese subalpine regions. Paper presented at IUFRO Symposium Carbon Uptake and Allocation in Subalpine Ecosystems as a Key to Management, Oregon State University, August 23, 1982.

KOYAMA, T., and FUJITA, N. 1981. Studies on *Abies* populations of Mt. Shimagare. I. Survivorship curve. Bot. Mag. **94**: 55–68.

KUETTNER, J. P. 1971. Cloud bands in the Earth's atmosphere: observations and theory. Tellus, **23**: 404–425.

MARDIA, K. V. 1970. A bivariate nonparametric C-sample test. J.R. Stat. Soc. Ser. B, **32**: 74–87.

MARDIA, K.V., and SPURR, B. D. 1973. Multisample tests for unimodal and axial circular populations. J.R. Stat. Soc. Ser. B, **35**: 422–436.

MOORE, F. R. 1980. A modification of the Rayleigh test for vector data. Biometrika, **67**: 175–180.

OSHIMA, Y., KIMURA, K., IWAKI, H., and KUROIWA, S. 1958. Ecological and physiological studies of the vegetation of Mt. Shimagare. I. Preliminary survey of the vegetation of Mt. Shimagare. Bot. Mag. **71**: 289–300.

ROBERTSON, A. 1986. Estimating mean windflow in hilly terrain from tamarack (*Larix laricina* (Du Roi) K. Koch) deformation. Int. J. Biometeorol. **30**(4): 333–349.

SETHURAMAN, S. 1979. Structure and turbulence over water during high winds. J. Appl. Meteorol. **18**: 324–328.

SPRUGEL, D. M. 1976. Dynamic structure of wave-regenerated *Abies balsamea* forests in northeastern United States. J.Ecol. **64**: 889–911.

——— 1985. Characteristics, causes and consequences of wave regeneration. *In* Establishment and tending of subalpine forests: research and management. *Edited by* H. Turner and W. Tranquilini. Proc. 3rd IUFRO Workshop, September 3–4, 1984. Eldg. Anst. forestl. Versuchswes., Ber. **270**: 179–188.

STEPHENS, M. A. 1962. Exact and approximate tests for direction I, II. Biometrika, **49**: 463–477, 547–552.

WEIHS, D. 1973. On the existence of multiple Karman vortex-street modes. J. Fluid Mech. **61**: 199–205.

WOODCOCK, A. H. 1940. Convection and soaring over the open ocean. J. Mar. Res. **5**: 248–253.

WOODCOCK, A. H., and WYMAN, J. 1947. Convective motion in air over the sea. Ann. N.Y. Acad. Sci. **48**: 749–777.